Rock and Soil Mechanics 2025 46(12): 3727−3739 ISSN 1000−7598
https: //doi.org/10.26599/RSM.2024.94300003 journal homepage: rocksoilmech.whrsm.ac.cn

Experimental investigation of the mechanical properties of counterpressure pile sheet retaining wall

GAN Fei[1, 2], WANG Shou-hong[1], ZHENG Gang[2], ZHOU Hai-zuo[2], LI Mei-lin[1], WANG Hong[1], BI Jing[1], ZHANG Yuan-yin[3]

1. School of Civil Engineering, Guizhou University, Guiyang, Guizhou 550025, China
2. School of Architectural Engineering, Tianjin University, Tianjin 300072, China
3. Guizhou Power Transmission and Transformation Limited Liability Company, Guiyang, Guizhou 550000, China

Abstract: The counterpressure pile sheet retaining walls are a novel type of slope support structure. Although engineering practice has demonstrated their excellent performance, systematic studies on their deformation characteristics and mechanical behavior remain limited. Through model tests comparing counterpressure piles and cantilever piles, this study investigates the evolution of pile-top displacement, pile deformation, internal force distribution, and earth pressure during the sandy backfill process. Key findings are as follows: (1) The top displacement of the cantilever pile was 81.76 mm, which is 6.69 times that of the counterpressure pile (12.22 mm), resulting in cracking in the soil mass 51 cm horizontally away from the pile top. (2) The counterpressure pile exhibits a typical S-shaped distribution of bending moment, with a distinct reverse bending phenomenon and a reduction in the peak moment. (3) The excessive deformation of cantilever piles leads to an increase in the gravitational component of soil weight perpendicular to the pile shaft direction. The soil pressure on the counter-pressure pile is about 15% lower than that on the cantilever pile, reflecting its good stress redistribution ability. (4) Three primary working mechanisms are identified: provision of anti-overturning moment through soil reaction on the counterpressure plate, enhancement of horizontal resistance via friction between the plate and soil, and increase of passive earth pressure in front of the pile. The counterpressure platform significantly enhances overturning resistance, mitigates slip, and improves long-term structural stability. These findings offer experimental validation and a theoretical basis for optimizing counterpressure pile sheet retaining wall designs.

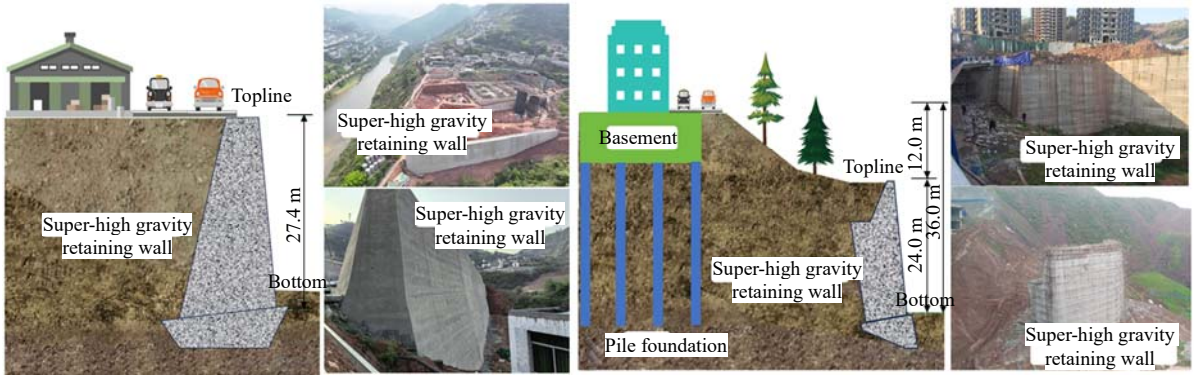
Keywords: counterpressure pile sheet retaining wall; model test; earth pressure; pile deformation; soil resistance in front of pile

1 Introduction

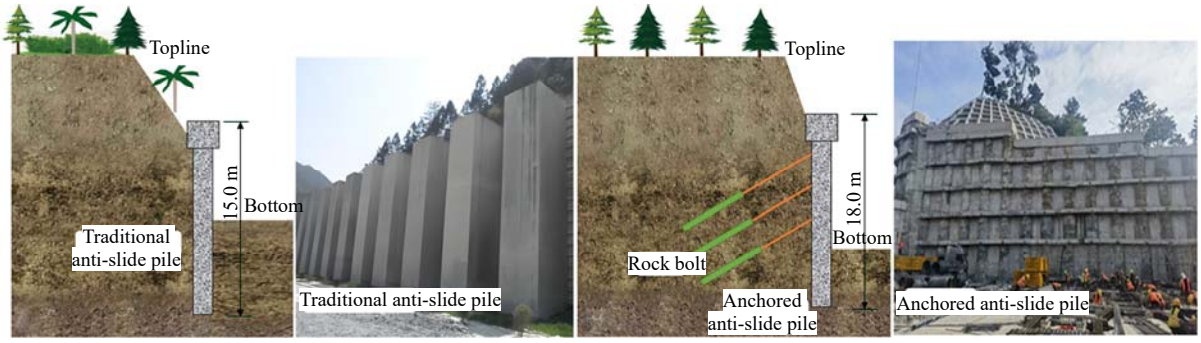
Retaining walls are widely used in engineering to counteract lateral earth pressure and prevent soil displacement or collapse behind structures[1−7]. Historically, three primary support structures were used in engineering: gravity retaining walls, anti-slip piles, and anchor pull piles (see Fig. 1). Each structure type has inherent limitations. Gravity retaining walls demand substantial materials and have height constraints, restricting their practical applications[8]. Anti-slip piles present operational challenges, including complex construction, extended project durations, high costs, and difficulties in controlling pile-top displacement. Anchor pull pile systems face spatial constraints as their anchor cable configurations often exceed construction boundary limits. The counterpressure pile-sheet retaining wall features an additional counterpressure platform at the slope's base in front of the pile (see Fig. 2). This design effectively redistributes the slope's load and enhances the pile's bending resistance[9]. This retaining wall offers a greater support height, lightweight design, and rapid construction. These advantages effectively mitigate slope deformation and structural instability[10]. As a result, this retaining wall has gained widespread recognition in both domestic and international engineering applications.

Advancements in high-fill slope reinforcement have driven notable progress in support structure technologies, particularly anti-slip piles and T-shaped pile systems. Anti-slip piles, as fundamental structural components, are widely applicable across diverse engineering scenarios. Zhang et al.[11] systematically investigated pile-soil interaction mechanisms and resistance coefficients using upper- and lower-bound analysis while exploring various geometric configurations. Liu et al.[12] employed Brillouin optical time domain reflectometry (BOTDR) to monitor deep-seated pile deformations and established a quadratic integral relationship between displacement and strain. To improve structural stability, researchers developed hybrid pile-anchor systems that mitigate slope displacement via synergistic reinforcement[13−15]. However, challenges in deformation monitoring and economic feasibility have prompted the search for alternative configurations. Current research focuses on T-shaped anti-slip piles and counter-weight pile-sheet retaining walls, which enhance monitoring accessibility and reduce implementation costs while maintaining structural efficiency. For instance, Ke et al.[16] conducted numerical simulations and introduced an equation based on plastic hinge positions to calculate

Received: 15 January 2025 Accepted: 22 April 2025
This work was supported by the National Natural Science Foundation of China (52164001, 52568047)
First author: GAN Fei, male, born in 1987, PhD, Associate Professor, mainly engaged in teaching and research in field of geotechnical mechanics. E-mail: fgan@gzu.edu.cn



(a) Super-high gravity retaining wall



(b) Traditional anti-slide pile (c) Anchored anti-slide pile

Fig. 1 Traditional types of slope support structures

the flexural load capacity of T-plate reinforced concrete composite shear walls. Won et al.[17] identified adequate stress levels in T-walls comprising H-piles and concrete walls through numerical modeling under realistic loading conditions, incorporating soil-structure interaction. Despite complex geological conditions, most studies focus on specific soil properties, which may undermine support structure stability[18]. The impact of soil property uncertainty on retaining wall stability, especially for pile-supported T-type retaining walls, remains insufficiently studied[19–21]. To address this gap, Zhang et al.[22–23] examined the effects of soil property uncertainty on T-type retaining wall stability using the random variable control method. Wang et al.[24] conducted low circumferential reverse loading tests on assembled T-column frames via numerical modeling to observe structural failure characteristics. They concluded that T-column frames are primarily affected by local compression, which negatively correlates with the wall-frame transverse stiffness ratio. Several scholars have conducted model tests to evaluate structural performance. Gao et al.[25] analyzed the seismic response of T-type retaining walls with liquefied foundations, comparing acceleration, displacement, earth pressure, and excess pore water pressure ratios in three model foundation soils and retaining walls. Kokkali et al.[26] observed through centrifuge testing that the maximum bending moment cross-section in new T-piles under filler weight occurs at one-third of the pile length. Wang et al.[27] and Zhang et al.[28] independently developed simplified calculation methods for soil resistance and the stability of inverted T-type conduit pile foundations. Finite element analysis revealed that the instability mode is rotational, centered around a point beneath the base plate and offset from the pile foundation axis. In previous studies, the use of gravity retaining walls, anti-slide piles, anchor piles, and other support structures has shown certain limitations. Key scientific issues, such as the load transfer path of counterpressure pile sheet retaining wall, the pile-soil-plate synergy mechanism, and the deformation evolution law of the structure, remain insufficiently understood.

In view of this, the counterpressure pile sheet retaining wall features convenient, efficient, and material-saving construction, while the counterpressure platform provides an anti-overturning moment. This study conducts a large-scale model test on the counterpressure pile sheet retaining wall and a cantilever pile. The variation characteristics of horizontal displacement, bending moment, axial force, shear force, and earth pressure during the layered backfilling process are analyzed and compared, verifying the structure's superior performance. The findings provide experimental data to support the practical application of the counterpressure pile sheet retaining wall.

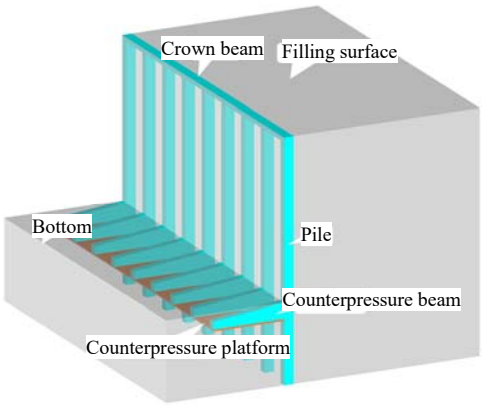


Fig. 2 Counterpressure pile sheet retaining wall

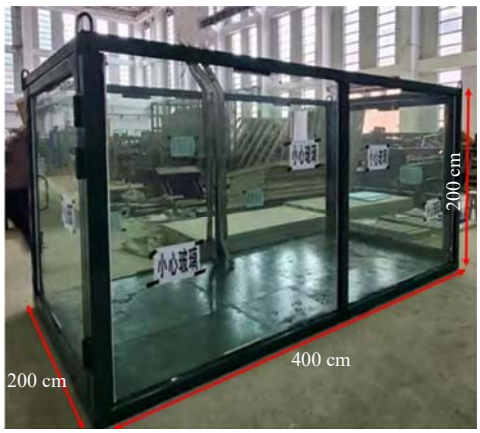


Fig. 3 The model box

2 Model test

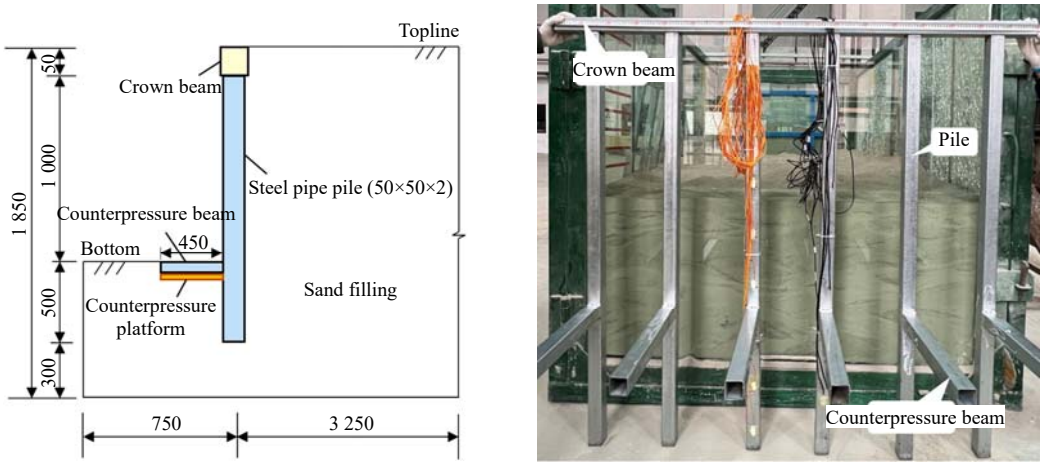
2.1 Overview of the experiment

This study investigates the mechanical behavior of counterpressure pile sheet retaining walls through comparative model tests with cantilever piles. The test model box measures 4 m×2 m×2 m (L×W×H), with a total volume of 16.0 m^3. It is constructed with a steel frame and transparent toughened glass. Sand was deposited using the sand-rain method with controlled buckets. Data collection was performed via a static strain gauge and a PC. Fig. 3 illustrates the model box.

2.2 Test materials

2.2.1 Anti-slide pile

References for the making of model piles [29−30]. As shown in Fig. 4, square steel pipe piles were used to simulate the supporting structure. Each pile measures 50 mm×50 mm in cross-section, with a wall thickness of 2 mm and a length of 150 cm. The supporting piles was positioned 750 mm from the model box end, with a spacing of 30 cm. The experiment was conducted simultaneously at both ends of the model box to compare the counterpressure pile sheet retaining wall and the cantilever pile. This arrangement minimized interference



(a) Schematic (unit: mm)

(b) Model pile

Fig. 4 The counterpressure piles

between the two structures, enhancing test efficiency. A total of 12 steel pipe piles were used, with leak-proof rubber skins placed behind them to simulate inter-pile slabs and prevent backfill leakage.

2.2.2 Crown beam

To analyze the internal force and deformation response of the counterpressure pile sheet retaining wall, the crown beam must provide adequate stiffness to ensure stability and structural integrity during testing. The crown beam measures 50 mm×50 mm in cross-section, with a wall thickness of 2 mm. Bolts are installed on the top of steel pipe piles to connect with the crown beam, ensuring effective stress transfer between the pile and the crown beam (see Fig. 4).

2.2.3 Test soil

The test used dry sandy soil extracted from Guiyang City, Guizhou Province, with a pre-filled volume of 14.4 m^3. Before filling, soil samples were collected, and shear

strength parameters—internal friction angle (φ) and cohesion (c)—were measured using a ZJ-type strain-controlled direct shear device. Laboratory tests were conducted to measure the relevant physical properties of the soil (see Table 1). The particle size distribution was analyzed using the sieving method (see Fig. 5), indicating a well-graded soil structure.

Table 1 Basic physical parameters of the test sand

G_s	d_{50} /mm	C_u	e_{min}	e_{max}	φ /(°)
2.71	0.281	2.4	0.796	0.564	38°

Note: G_s is the specific gravity; d_{50} is the mean particle size; C_u is the coefficient of uniformity; e_{min} and e_{max} are the minimum and maximum void ratios, respectively; and φ is the peak internal friction angle.

2.3 Monitoring systems

(1) Strain gauges: The strain gauges were symmetrically arranged on the cross-section of the supporting pile, as shown in Fig. 6(b).

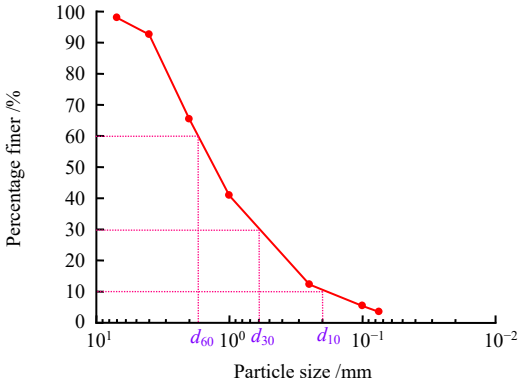
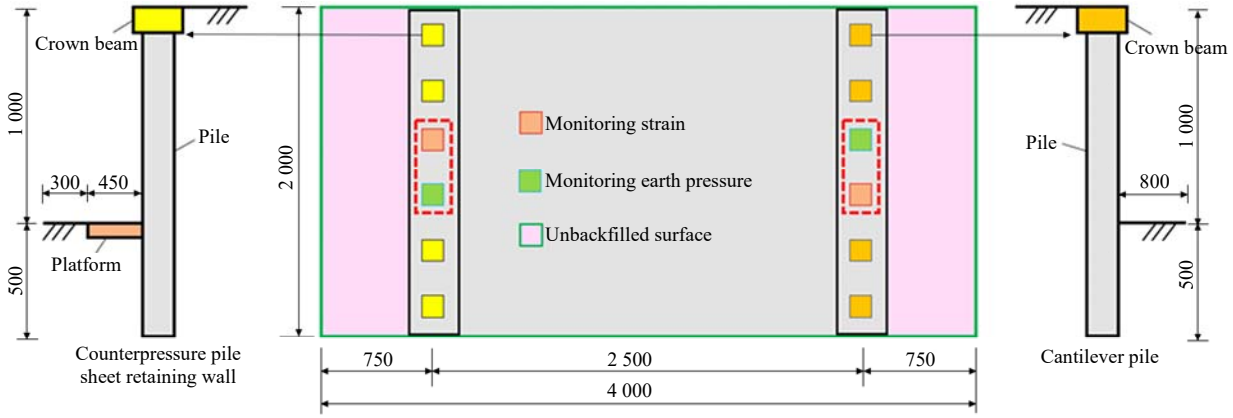
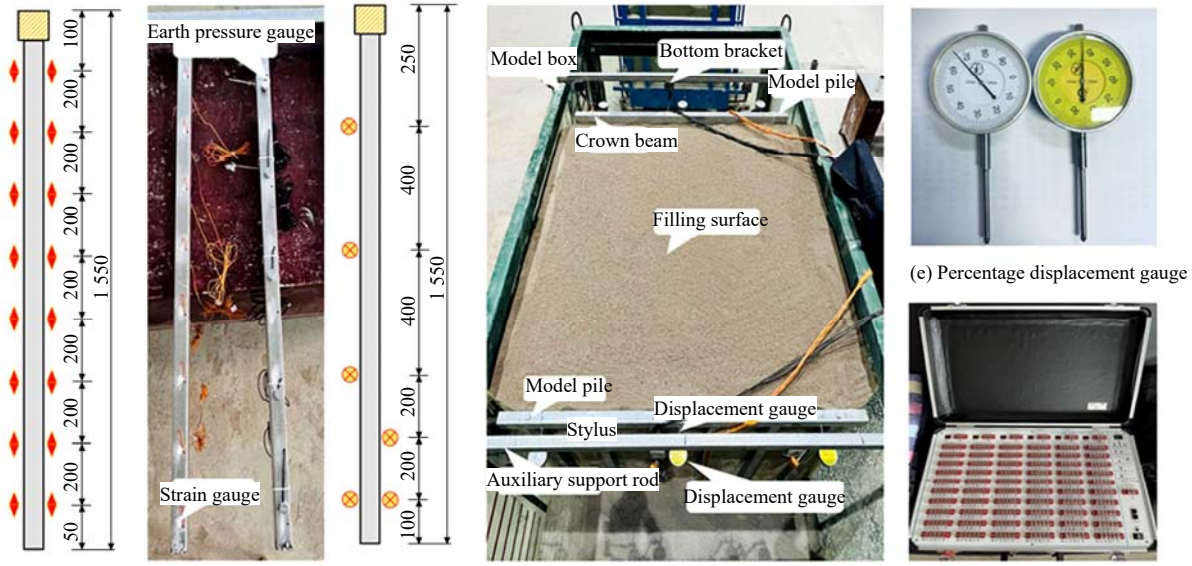


Fig. 5 Grain size distribution of sand



(a) Schematic diagram of pile earth pressure and strain monitoring



(b) Strain gauge layout (c) Earth pressure gauge layout (d) Percentage table layout (e) Percentage displacement gauge (f) Strain gauge

Fig. 6 Schematic arrangement of test sensors (unit: mm)

(2) Miniature earth pressure box: This test monitored the active earth pressure behind the pile, the passive earth pressure in front of the pile, and the earth pressure distribution beneath the counterpressure platform. The

diameter of the earth pressure box was 27.0 mm, with a measuring range of 0 to 0.6 MPa. The arrangement is shown in Fig. 6(c).

(3) Electronic displacement sensors: To monitor the top pile displacement and horizontal displacement of the test pile, six electronic displacement sensors were fixed at the left, center, and right positions of the crown beam on top of the pile, as shown in Fig. 6(d), after the pile was laid.

(4) Electronic static strain gauge (uT7130): The maximum range of the strain gauge was $\pm 3\times10^{-2}$, with a measurement precision of 0.1×10^{-6} and a measurement error of ±1‰, as shown in Fig. 6(f).

2.4 Experimental steps

When the pile and monitoring device installation is complete, all the connecting wires into the strain gauge, equipment debugging, to ensure that the equipment is normal to start sand backfilling, filling steps are as follows:

(1) A crane device was used to transfer two groups of assembled test piles to the calibrated position of the model box. The sand was then added using the sand and rain method to fill the soil up to 30 cm from the bottom of the model box. A sand compaction treatment was applied as the bedding layer for the test pile. During the filling process, the test pile was lifted to the predetermined height, ensuring that the bottom of the pile was 30 cm above the bottom of the box.

(2) After the completion of the bedding fill, the sand was continued to be added up to 80 cm from the bottom of the model box (the location of the counterpressure platform). Subsequently, the installation of the counterpressure plate was carried out. Once all the test piles were in place, an electronic displacement sensor was fixed to the crown beam to monitor the displacement of the pile tops in preparation for the subsequent slope backfilling test.

(3) After installing all piles, no additional sand was placed in front, and filling continued behind the piles. After a 2-hour stabilization period, initial percentage readings and pile strain measurements were recorded. The soil was then placed and compacted in 30 cm layers, ensuring uniform filling and compaction. Precautions were taken to prevent direct contact between the sand and the earth pressure box or strain gauges, ensuring accurate instrument positioning and readings. Each sand layer was leveled after filling. Each backfill layer settled for 2 hours before data collection to ensure soil stabilization. The process was repeated until the full load was reached. Upon reaching full capacity, final instrument readings were recorded. Fig. 7 illustrates the test fills.

3 Analysis of results

3.1 Displacement analysis

3.1.1 Pile top displacement

After each backfilling stage was left to settle for 2 hours, the readings of the three dial gauges at the left, center, and right positions were recorded, and the average value was taken as the horizontal displacement of the pile top. Fig. 8 presents the curve of horizontal displacement versus backfilling height.

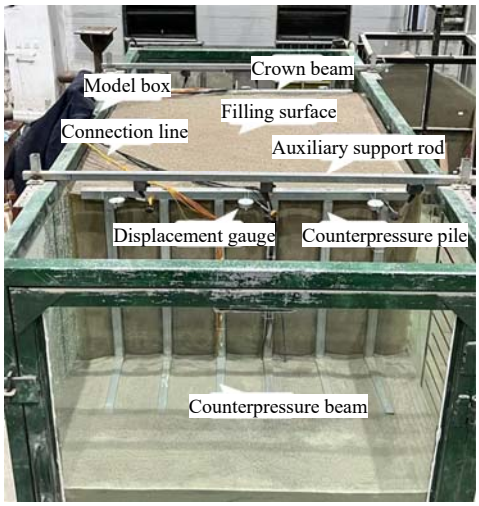


Fig. 7 Test soil fill diagram

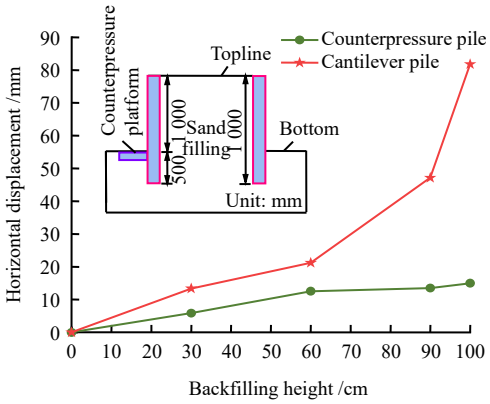
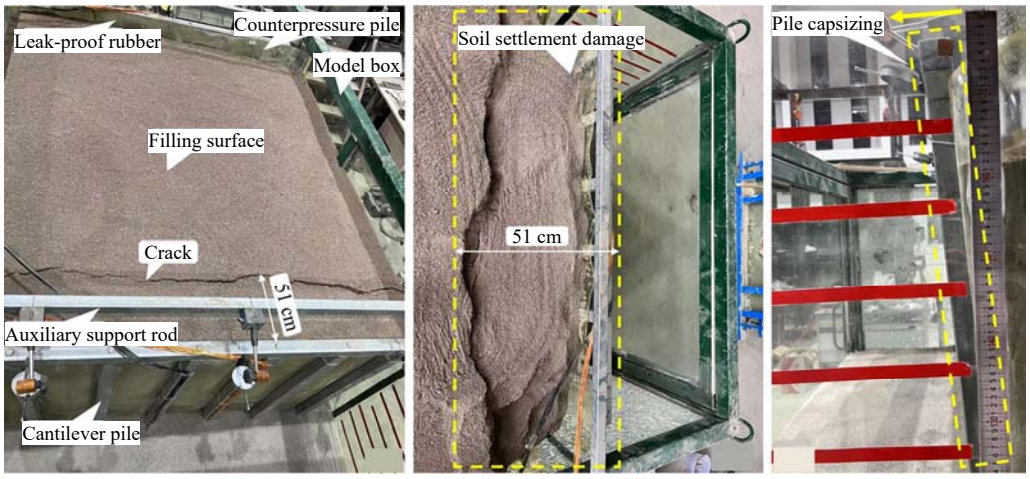


Fig. 8 Horizontal displacement curves of pile top

As shown in Fig. 8, the horizontal displacement of both counterpressure and cantilever pile tops increased with backfilling height. The cantilever pile displacement rate increased progressively during backfilling, with a sharp rise at 90 cm, where a distinct damage inflection occurred. In contrast, the counterpressure pile top displacement initially increased rapidly, then decelerated, and eventually stabilized. During backfilling, the cantilever pile top displacement consistently exceeded that of the counterpressure pile, with the difference increasing as backfilling height rose.

At a backfilling height of 30 cm, the counterpressure pile top displacement was minimal, while the cantilever pile top displacement reached 13 mm, 2.27 times greater. The displacement growth rates for the counterpressure and cantilever piles were 19.63% and 44.56%, respectively. Between 30 cm and 60 cm backfilling height, both structures exhibited similar displacement growth rates. When the

backfilling height reached 100 cm, the cantilever pile top displacement increased significantly, reaching 21.22 mm, 47 mm, and 81.76 mm, with corresponding growth rates of 86.39% and 346.3%. In contrast, the counterpressure pile displacement growth rate slowed, with values of 12.56 mm, 13.52 mm, and 14.99 mm and corresponding growth rates of 3.21% and 14.7%. At 100 cm backfilling height, the counterpressure pile top displacement was only 18.3% of the cantilever pile's displacement. The soil above the counterpressure pile showed no significant settlement, whereas the soil above the cantilever pile exhibited cracking and settlement damage (see Fig. 9(b)), with substantial tipping deformation (see Fig. 9(c)). The cracking location in the upper soil of the cantilever pile was 51 cm from the pile top, and the actual rupture angle of the sandy soil was calculated as 63°. According to Rankine's earth pressure theory, the rupture angle should be 64.0°, with a slight deviation due to differences between theoretical assumptions and actual conditions. Figure 9 shows that the soil behind the counterpressure pile remained intact, confirming its effectiveness in controlling pile-top horizontal displacement.



(a) Soil cracking (b) Soil settlement (c) Pile overturning

Fig. 9 Soil cracking, settlement at the top surface of cantilever pile and pile overturning deformation

3.1.2 Pile displacement

The displacement curve of the supporting pile can be determined from the strain values monitored at symmetric sections of the pile. The angle of rotation and deflection are calculated based on the axial strain difference ($\Delta\varepsilon$) measured between two points in each pile section. Assuming a linear distribution of strain differences between adjacent test sections, the pile is divided into 8 segments from the bottom to the top. Consequently, the strain difference at 20 cm within each of the 8 segments is:

$$\Delta\varepsilon = \Delta\varepsilon_i + \frac{\Delta\varepsilon_{i+1} - \Delta\varepsilon_i}{l_i} x \tag{1}$$

where $\Delta\varepsilon$ is the axial strain difference, $\Delta\varepsilon_i$, $\Delta\varepsilon_{i+1}$ are the bending strains of section i, i+1, respectively; l_i is the length of pile unit i. The relationship between the Integrating equation (2) once yields the rotation angle θ_(i+1) at each cross-section. Integrating equation (3) twice provides the deflection y_(i+1) for each surface, i.e., lateral displacement y of the pile section and the turning angle θ is:

$$\frac{\mathrm{d}^2 y}{\mathrm{d}x^2} = \frac{\mathrm{d}\theta}{\mathrm{d}x} = \frac{M}{EI} \tag{2}$$

where EI is the bending stiffness of the pile, E is the modulus of elasticity of the steel pipe pile; I is the moment of inertia of the pile section; and M is the bending moment of the pile. From Eqs. (1), (2) we can get:

$$\frac{\mathrm{d}^2 y}{\mathrm{d}x^2} = \frac{1}{b_0}\left(\Delta\varepsilon_i + \frac{\Delta\varepsilon_{i+1} - \Delta\varepsilon_i}{l_i} x\right) \tag{3}$$

where b_0 is the effective calculated width of the pile.

Integrating Eq. (2) once yields the rotation angle θ_{i+1} at each cross-section. Integrating Eq. (3) twice provides the deflection y_{i+1} for each surface, i.e.,

$$\left.\begin{aligned} \theta_{i+1} &= \theta_i + \frac{l_i}{2b_0}\left(\Delta\varepsilon_{i+1} + \Delta\varepsilon_i\right) \\ y_{i+1} &= y_i + \theta_i l_i + \left(\Delta\varepsilon_{i+1} + 2\Delta\varepsilon_i\right)\frac{l_i^2}{6b_0} \end{aligned}\right\} \tag{4}$$

The horizontal displacement curve of the pile shaft can be obtained through double integration, as shown in Fig. 10. Pile displacement increases with backfilling height, though notable variations exist in its distribution. Between 0 cm and 60 cm backfilling height, the cantilever pile displacement increased at a nearly constant rate with a stable increment. However, beyond 60 cm backfilling height, the pile displacement growth rate accelerated, with the pile-top horizontal displacement increasing by 73.5% between 90 cm and 100 cm. This led to soil collapse and failure behind the pile. As shown in Fig. 10(b),

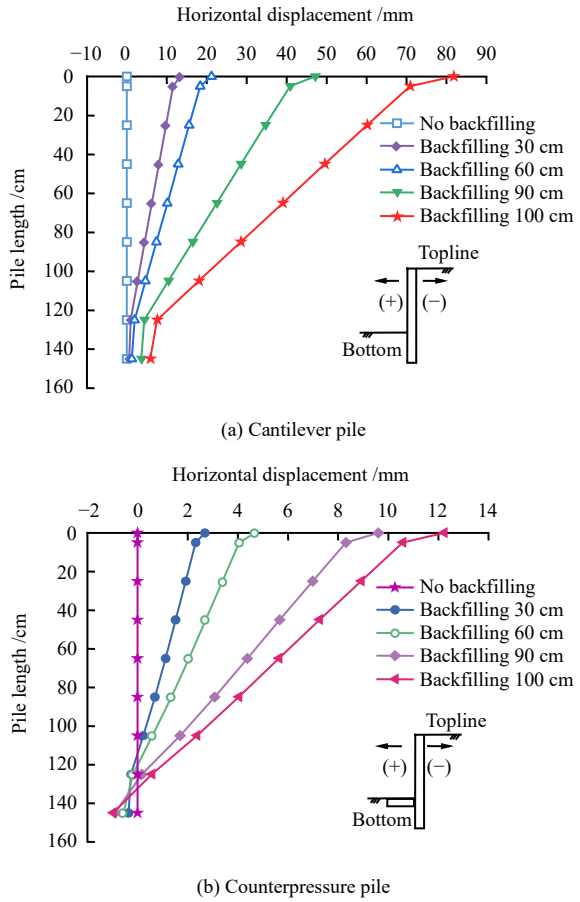


Fig. 10 Horizontal displacement curves of pile

the counterpressure pile displacement evolution resembles that of the cantilever pile at the same backfilling height but with smaller differences. Notably, displacement growth accelerates between 60 cm and 90 cm backfilling height. Negative horizontal displacement at 120 cm depth indicates pile-top forward tipping and bottom backward tilting. The counterpressure platform compresses the lower rock and soil mass, generating an upward reactive force that provides an anti-slumping moment, limiting pile backward movement. Simultaneously, the counterpressure platform's soil reaction force increases passive earth pressure, further amplifying the overturning moment. This enhances the pile's overturning safety factor and reduces overall horizontal displacement.

3.2 Earth pressure analysis

Figure 11 shows the earth pressure variation at different locations on the counterpressure and cantilever piles during backfilling. A detailed analysis is provided below: (1) Variation with depth: With increasing depth, the earth pressure in the active zone behind the pile shows a nonlinear pattern, initially increasing and then decreasing. In contrast, the Rankine earth pressure curve exhibits a linear increase. The measured earth pressure values deviate from the Rankine theoretical values due to the differences between the idealized assumptions of Rankine earth pressure and the actual soil conditions. During the test, the ratio of pile-top displacement to wall height was Δ/H = 1% for

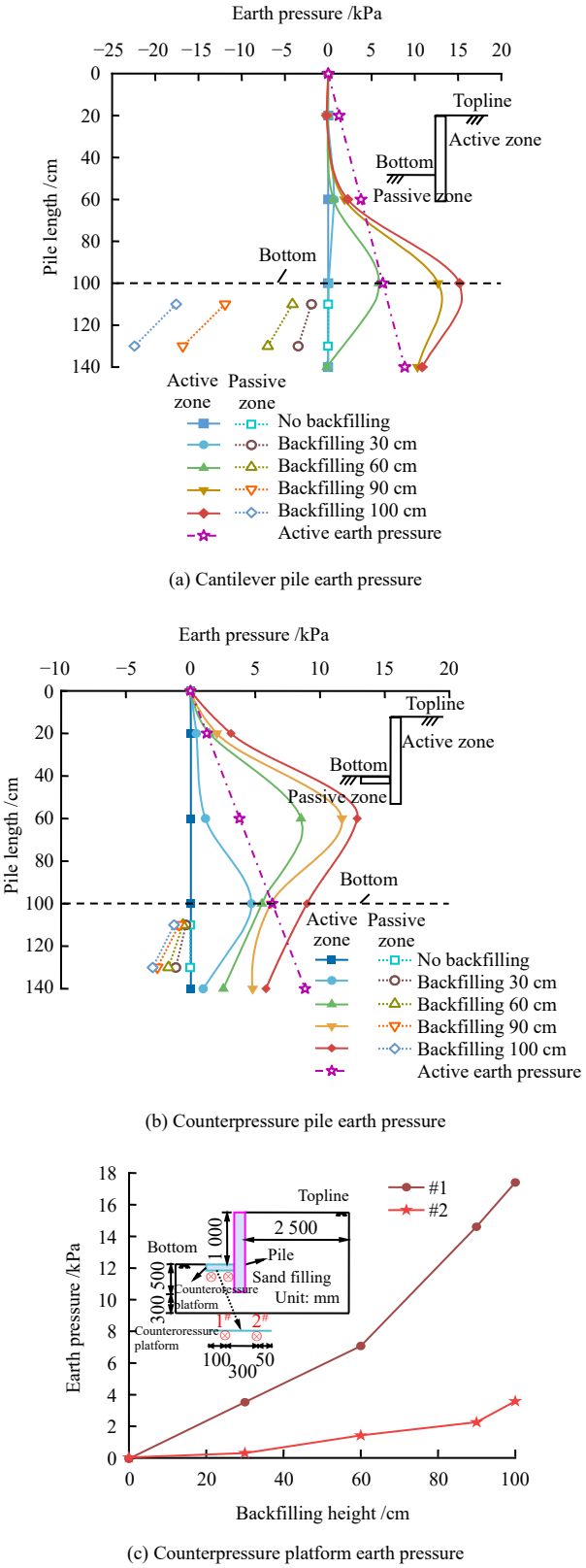


Fig. 11 Variation curves of earth pressure with backfilling height of slope

the counterpressure pile and Δ/H = 8% for the cantilever pile. Both values exceed the displacement required for the soil behind the wall to reach the active limit equilibrium state (Δ/H = 1‰–5‰) [28]. This indicates that the soil had already reached the active limit state, resulting in

the measured earth pressures being higher than the theoretical predictions. (2) Active earth pressure: The active earth pressure behind the pile increases as the backfilling height rises. In cantilever piles, the earth pressure change is more pronounced in the lower half of the pile, with the maximum value occurring at approximately 2/3 of the pile length. In counterpressure piles, however, the maximum earth pressure points shift upward as backfilling progresses, reaching the pile midpoint upon completion. As backfilling height increases, the pile tilts, relaxing the sandy soil at its base. This relieves stress and reduces earth pressure at the lower pile section. After backfilling, the maximum earth pressure reaches 15.18 kPa for the cantilever pile and 12.88 kPa for the counterpressure pile, a 15% reduction. (3) Passive earth pressure: The passive earth pressure in front of the pile increases with backfilling height. When backfilling reaches 60 cm, passive earth pressure in front of the counterpressure pile stabilizes. Further backfilling induces tipping, increasing deformation at the counterpressure platform's front end while reducing deformation near the pile bottom. This leads to negative displacement at the pile base and soil relaxation. The deformation required for the support reaction force at the pile base and friction at the lower counterpressure platform end is much smaller than that required for passive earth pressure, weakening the passive earth pressure and causing only minor variations. (4) Earth pressure distribution on the counterpressure platform: Fig. 11(c) shows that earth pressure data from counter-pressure platforms #1 and #2, along with their differential values, increase with backfilling height. Earth pressure at measurement point #1 exceeds that at point #2, indicating that the support reaction force at the pile base increases with distance from the pile. After backfilling, earth pressure at point #1 is 17.4 kPa, while at point #2, it is 3.6 kPa, a difference of 13.8 kPa. The counterpressure platform enhances passive earth pressure by redistributing it in front of the pile. Additionally, the base reaction force generates an anti-tilting moment, reducing soil deformation and improving the retaining wall's bending performance and stability.

As shown in Fig. 11(a) and 11(b), the earth pressure curves of both counterpressure and cantilever piles intersect with the Rankine earth pressure curves, indicating that the soil behind the pile reaches the active limit equilibrium state, where measured earth pressure values align with calculated ones. As backfilling progresses, the counter-pressure platform's support reaction force counteracts slope thrust in front of the pile, reducing lower pile deformation and promoting active limit equilibrium near the pile base. As overturning progresses, the cantilever pile induces soil relaxation at its base, hindering the maintenance of active limit equilibrium and leading to fewer intersections between the earth pressure curve and the calculated values.

3.3 Internal forces of pile

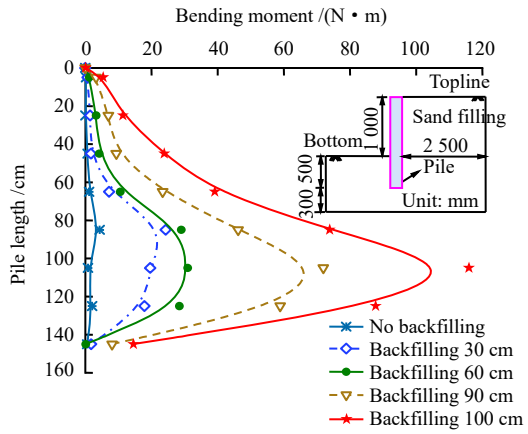
3.3.1 Bending moment distribution of pile

The bending moment value of the pile shaft at each backfill height can be calculated using the tensile and compressive strain values on both sides of the pile shaft according to the following formula. The corresponding bending moment distribution curves for different pile types are shown in Fig. 12.

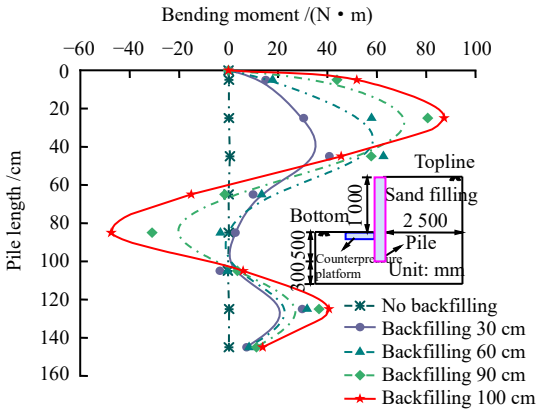
$$M = EI\frac{\varepsilon_1 - \varepsilon_2}{y} \tag{5}$$

where ε_1, ε_2 are the tensile and compressive strain values of the pile, respectively.

Figure 12(a) shows that the cantilever pile's bending moment follows a "fish-belly" distribution, gradually increasing with backfilling height and accelerating at each step. At 100.0 cm backfilling height, the maximum bending moment reaches 115.0 N • m, occurring at 105.0 cm from the pile top. Fig. 12(b) shows that the counterpressure pile's bending moment follows an S distribution, increasing with backfilling height and accelerating at each step. At 30.0 cm backfilling height, the maximum bending moment is 40.8 N • m at 45.0 cm from the pile top. At 60.0 cm, it increases to 62.7 N • m at the same section. At 90.0 cm, the maximum bending moment reaches 80.6 N • m, with the peak shifting to 25.0 cm from the pile top. At 100.0 cm backfilling height, the maximum bending moment is 87.2 N • m, occurring at 25.0 cm from the pile top. At this stage, the counterpressure pile's maximum bending moment is 75.8% of the cantilever piles. As backfilling height increases, the maximum bending moment section of the counterpressure pile gradually shifts upward, moving from the bottom toward the pile top. Two distinct "counter-bending" phenomena occur in the pile. The base reaction force and frictional resistance generated by the counterpressure platform create an anti-overturning moment that acts in opposition to the earth pressure on the pile. This opposition counteracts the overturning moment induced by the earth pressure behind the pile, reversing the direction of the bending moment. The bending moment becomes dispersed into multiple extreme values, with the maximum value reduced by 24.17%. The rebound point in the upper half shifts upward with increasing backfilling, whereas the rebound point near the counterpressure platform remains relatively unchanged. A negative bending moment peak appears at 85 cm from the pile bottom, followed by a decrease in bending moment with depth. This results from the base reaction force generated by soil compression at the lower end of the counterpressure platform, causing a sudden shift in pile position. The base reaction force counteracts slope thrust, reducing the bending moment and altering the typical "fish-belly" distribution seen in traditional cantilever piles.



(a) Bending moment of cantilever pile



(b) Bending moment of counterpressure pile

Fig. 12 Variation curves of pile bending moment with backfilling height

Figure 12 shows that the counterpressure pile experiences smaller bending moments than the cantilever pile. During backfilling, the soil in front of the cantilever pile undergoes relaxation and stress release, weakening its restraining effect. Meanwhile, the earth pressure behind the pile increases due to soil self-weight, resulting in a higher bending moment. The counterpressure platform redistributes stress on the cantilever pile, while counterforce from the lower foundation allows soil near the pile base to reach stress equilibrium earlier on both sides of the pile. Consequently, the counterpressure pile exhibits superior support performance compared to the cantilever pile. The counterpressure platform restricts pile rotation and lateral displacement while reducing bending moments, thereby minimizing deformation and enhancing structural stability.

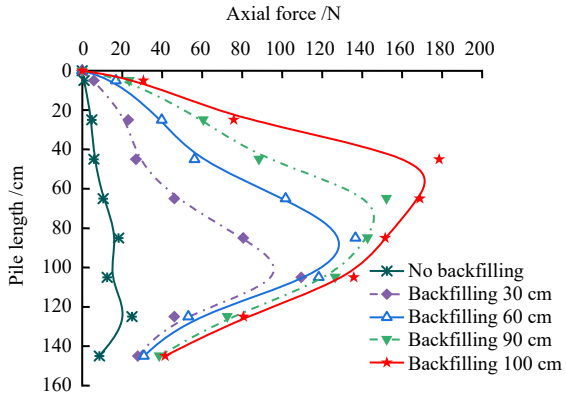
3.3.2 Distribution of pile axial force

Based on the strain values of the supporting pile monitored by the strain collector, the axial force of the pile during the backfilling process was calculated according to the following formula.

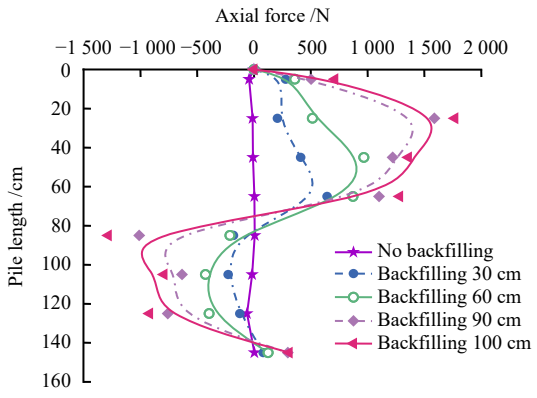
$$N = \frac{\varepsilon_1 + \varepsilon_2}{2} EA \tag{6}$$

where N is the axial force of the pile; and A is the cross-section.

Figure 13(a) shows that the cantilever pile primarily experiences tension, with its axial force following a "fish-belly" distribution—initially increasing and then decreasing. As backfilling height increases, the axial force gradually rises, with the peak position shifting upward and the growth rate stabilizing. The maximum axial force reaches 178.6 N. The low friction factor between the sandy soil and the steel pipe pile, along with the nearly horizontal earth pressure behind the pile, results in a relatively small axial force. Figure 13(b) shows that the upper pile section is in tension, while the lower section is in compression, forming an S-shaped axial force distribution. The axial force near the pile bottom approaches zero due to partial counteraction by upward soil friction below the peak axial force. As backfilling height increases, the counterpressure pile's axial force also rises, with the peak position shifting upward accordingly. The maximum axial force reaches 1 767.2 N. The counterpressure pile experiences greater axial force than the cantilever pile, mainly due to the support reaction force from the soil at the lower counterpressure platform, which generates additional radial force on the pile. This induces greater soil extrusion and deformation near the pile bottom, causing the embedded section to displace downward relative to the soil, thereby increasing axial force in the counterpressure pile.



(a) Axial force of cantilever pile



(b) Axial force of counterpressure pile

Fig. 13 Axial force curves of pile as a function of backfilling height

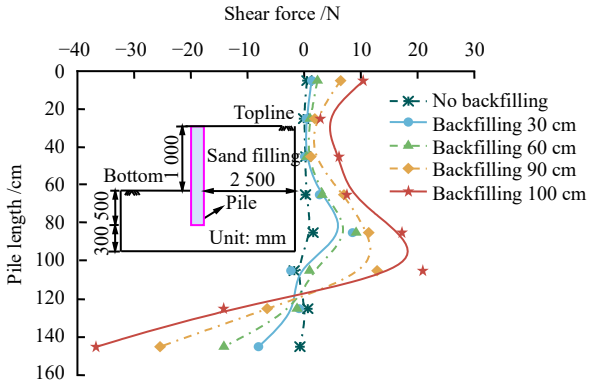
3.3.3 Shear force distribution of pile

According to the theory of material mechanics, the shear force of a pile can be obtained by taking the first derivative of the bending moment, with the expression as follows:

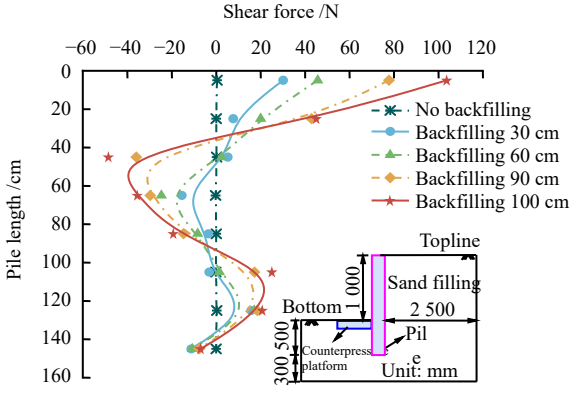
$$Q = \frac{\mathrm{d}M}{\mathrm{d}x} \tag{7}$$

where Q is the shear force of the pile.

Figure 14(a) shows that the shear force along the cantilever pile depth increases with backfilling height, with its growth rate gradually accelerating. After backfilling, the shear force decreases before increasing, peaking at 21.05 N near the slope's bottom. Beyond the peak, the shear force rapidly drops to zero at 120 cm along the pile and then reverses direction. This occurs due to the base reaction force from soil extrusion at the pile's lower end, causing a sudden shear force shift that counteracts the earlier slope thrust. As backfilling height increases, the shear distribution and peak stress location remain unchanged. Fig. 14(b) shows that the counterpressure pile's shear force follows an S distribution, increasing with backfilling height as its growth rate accelerates. During backfilling, three zero-shear points emerged, and the pile's maximum stress point gradually shifted upward with increasing backfilling height. After backfilling, the pile reaches shear force peaks at 45 cm (−48.3 N) and 110 cm (25.2 N), with 103.9 N at the top. Shear force variations mainly occur within the 0−100 cm section, with minimal changes below the counterpressure platform. The counterpressure platform supports most of the load, restricts pile overturning, and enhances structural stability.



(a) Shear force of cantilever pile



(b) Shear force of counterpressure pile

Fig. 14 Shear force curves of pile as a function of backfilling height

3.4 Working mechanism of counterpressure pile sheet retaining wall

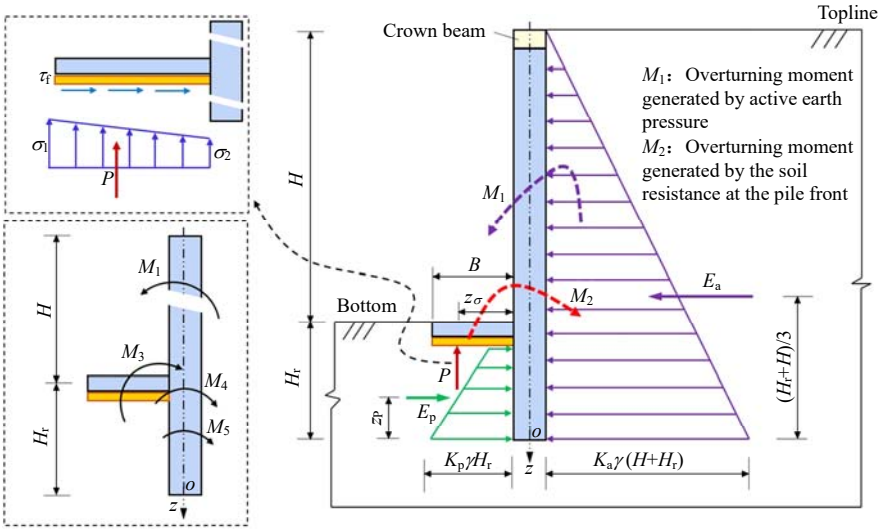
The mechanical mechanism of the counterpressure pile sheet retaining wall is illustrated in Fig. 15, with its primary effects highlighted in the following three aspects: (1) Providing anti-tilting moment. The counterpressure platform rotates with the overturning deformation of the pile, compressing the rock and soil at the lower end to generate an upward vertical force. This force provides an anti-tilting moment to the pile, thereby enhancing its overall bending resistance. When the strength of the rock and soil mass beneath the counterpressure platform is high, the retaining wall's performance is significantly improved. (2) Providing frictional resistance(τ_f). The counterpressure platform contacts the soil in front of the pile, offering horizontal resistance. The interaction between the pile and soil increases the passive earth pressure, contributing to the overall resistance. (3) Increasing soil resistance in front of the pile: The vertical force (P), frictional resistance(τ_f), and increased passive earth pressure collectively enhance the soil resistance in front of the pile, thereby increasing the pile's overturning moment.

As shown in Fig. 15, the vertical force distribution is trapezoidal, and the anti-tilting moment M_3 is generated by the vertical force of the lower part of the counterpressure platform, the anti-tilting moment M_4 is generated by the frictional resistance, and the anti-tilting moment M_5 is generated by the passive earth pressure. The overturning moment produced by the soil resistance in front of the pile is the overturning moment produced by the combination of vertical force, frictional resistance, and passive earth pressure, i.e., $M_2 = M_3+M_4+M_5$. The overturning resistance of the counterpressure pile shows good adaptability and can effectively cope with complex soil deformation and external forces to ensure the long-term stability of the structure.

4 Discussion

This study compares the mechanical behavior and performance of cantilever and counterpressure piles during backfilling through indoor model tests. However, limitations in funding, manpower, and experimental conditions have led to certain deficiencies requiring further investigation.

(1) Model size and similarity ratio: The test was conducted in a 400 cm×200 cm×200 cm (L×W×H) model box with predetermined similarity ratio parameters.



Note: H and H_r are the slope height and the embedded depth of the retaining section, respectively; E_a and E_p are the active earth pressure and passive earth pressure, respectively; K_a and K_p are the coefficients of active and passive earth pressure, respectively; z_a, z_p, and z_σ are the action points of the active earth pressure, passive earth pressure, and the soil reaction force on the counterpressure platform, respectively; γ is the soil unit weight; τ_f is the frictional resistance along the base of the counterpressure platform; P is the reaction force exerted by the soil on the counterpressure platform; and B is the length of the counterpressure platform.

Fig. 15 Working mechanism diagram of counterpressure pile

However, boundary effects and limited soil volume restricted the accurate representation of gravitational effects. Future studies should reduce the similarity ratio or conduct full-scale engineering tests to improve experimental accuracy.

(2) Soil conditions: To highlight the load-bearing characteristics of the supporting piles, a homogeneous sandy soil was used as the testing medium. This idealized condition helps to clarify the pile–soil interaction mechanism, but it still differs from the complex geological conditions encountered in practical engineering. Future research should consider groundwater seepage and saturated sandy soil conditions to improve practical applicability and engineering relevance.

(3) Simulation of construction processes: Hollow steel pipe piles were used to simulate micropiles; however, key construction processes, such as high-pressure grouting and barbed protection, were not included. Future experiments should enhance process simulation to better reflect real construction conditions.

(4) The research emphasizes the comparative verification of structural forms rather than the precise extrapolation of specific engineering parameters. Consequently, the similarity criterion is not strictly adhered to in the scale design. Future studies will further investigate the similarity ratio issue through centrifuge experiments or numerical simulations.

(5) The discussion on the working mechanism of the counterpressure pile sheet retaining wall in this study remains largely qualitative, and a comprehensive theoretical analysis system has yet to be established. Significant gaps persist regarding the mechanism and quantitative characterization of the frictional resistance at the interface between the counterpressure platform and the soil. Given the critical role of interfacial friction resistance and the anti-overturning moment in the overall structural stability, future research should prioritize developing a mechanical analysis model for the structural system.

5 Conclusion

This paper presents a model test study on the counter-pressure pile sheet retaining wall to examine the deformation, earth pressure, and internal force evolution during the backfilling process of the supporting structure. The key conclusions are drawn as follows:

(1) The horizontal displacements of both the pile top and the pile shaft of cantilever piles and counterpressure piles increase with the increase in backfill height, and the displacement of the pile shaft of counterpressure piles is significantly smaller than that of cantilever piles. After backfilling is completed, the displacement of the pile top of the cantilever pile is 81.76 mm, which is 6.69 times that of the counter-pressure pile (12.22 mm), resulting in significant settlement damage to the soil at the top of the slope.

(2) The bending moment diagram of the cantilever pile exhibits a “fish-belly” distribution, while the counter-pressure pile displays a S distribution pattern, with a notable counter bending phenomenon observed in the upper part of the pile. Upon completion of backfilling, the maximum bending moment for the counterpressure pile is 87.2 N • m, while for the cantilever pile, it is 115.0 N • m. The maximum bending moment of the

counterpressure pile is 75.8% of that of the cantilever pile.

(3) The active earth pressure for both the counterpressure pile and the cantilever pile initially increases and then decreases with depth. Upon completion of backfilling, the maximum earth pressure for the cantilever pile is 15.18 kPa, while that for the counterpressure pile is 12.88 kPa, representing a decrease of approximately 15%. Furthermore, the earth pressure and its difference in the lower part of the counterpressure platform increase with the backfilling height.

(4) The counterpressure pile supporting structure operates through three main mechanisms: providing anti-tilting moment, offering horizontal resistance, and increasing soil resistance in front of the pile. The interaction of these mechanisms enhances the overturning resistance of the counterpressure pile, enabling it to effectively withstand complex soil deformations and external forces, thereby ensuring the long-term stability of the structure.

References

[1] QI Y, XIAO S G. Calculation method for static and seismic active earth pressure on counterweight retaining walls under translation based on two critical slip surfaces[J]. Transportation Geotechnics, 2024, 48: 101349.

[2] CHEN H X, WANG M Y, WANG S, et al. Internal variable gradient model for active earth pressure of rigid retaining wall moving with translation[J]. Geohazard Mechanics, 2024, 2(3): 189−196.

[3] ZHENG G, GUO Z Y, ZHOU H Z, et al. Multibench-retained excavations with inclined–vertical framed retaining walls in soft soils: observations and numerical investigation[J]. Journal of Geotechnical and Geoenvironmental Engineering, 2024, 150(5): 5024003.

[4] JIANG J F, ZHAO Q H, ZHU S R, et al. Arching effect and displacement on theoretical estimation for lateral force acting on retaining wall[J]. Natural Hazards, 2021, 108(3): 2991−3019.

[5] HOU Tian-shun, YANG Kai-xuan. Model test on earth pressure at rest of light weight soil mixed with EPS particles behind a retaining wall[J]. Rock and Soil Mechanics, 2021, 42(12): 3249−3259, 3270.

[6] ZHENG Jun-jie, SHAO An-di, XIE Ming-xing, et al. Experimental study on retaining wall with EPS cushion under different backfilling widths[J]. Rock and Soil Mechanics, 2021, 42(2): 324−332.

[7] ZOU Wei-lie, LENG Jian-jun, WANG Xie-qun. Numerical analysis of working properties and earth pressure calculation of geosynthetic-reinforced soil gravity retaining wall[J]. Rock and Soil Mechanics, 2011, 32(Suppl.2): 70−75.

[8] XIONG C X, XU Y Y, XING Z Q, et al. Study on active earth pressure of narrow backfilling of balance weight retaining wall under translational displacement mode[J]. Developments in the Built Environment, 2024, 18: 100430.

[9] ZHU Lei, XIA Cheng-zhi, XIE Peng, et al. Application of T type anti slide pile in landslide treatment[J]. Journal of Hubei University of Technology, 2021, 36(1): 88−93.

[10] CHATTERJEE J, AMINI F. Slope stability modeling and analysis of T-wall subjected to hurricane loading[J]. International Journal of Geotechnical Engineering, 2011, 5(1): 103−112.

[11] ZHANG Wei-min, GU Xing-wen. Ultimate lateral resistance of piles with different section shapes[J]. Chinese Journal of Rock Mechanics and Engineering, 2020, 39(Suppl.2): 3526−3537.

[12] LIU Yong-li, SUN Hong-yue. Research on deformation monitoring and determination[J]. Chinese Journal of Rock Mechanics and Engineering, 2013, 32(10): 2147−2153.

[13] LING Y Q, SONG L, HAO J, et al. Analytical analysis for horizontal displacement of pile anchor support structure considering prestress[J]. Frontiers in Ecology and Evolution, 2023, 11: 1249239.

[14] JAIN S K, NUSARI M S, SHRESTHA R, et al. Use of RCC pile, anchor bolt, and geogrid for building construction on the unstable slope[J]. Geoenvironmental Disasters, 2023, 10: 13.

[15] AAMER F, AZZAM W, FAROUK A, et al. Utilization of blade anchor for improving the uplift capacity of pile in sand: model study[J]. Ocean Engineering, 2023, 278: 114435.

[16] KE X J, LIU L Z, CHEN S J, et al. Study on bearing capacity of T-shaped steel plate reinforced concrete composite shear wall[J]. Structures, 2024, 67: 107022.

[17] WON J, ADHIKARI S, SONG C R, et al. Evaluation of a T-wall section in New Orleans considering 3D soil-structure interaction[J]. Journal of Geotechnical & Geoenvironmental Engineering, 2011, 137(8): 731−742.

[18] HUANG L C, HUANG S, LAI Z S. On the optimization of site investigation programs using centroidal Voronoi tessellation and random field theory[J]. Computers and Geotechnics, 2020, 118: 103331.

[19] RAJABALINEJAD M, GELDER P H A J M V, DEMIRBILEK Z, et al. Application of the dynamic bounds method in the safety assessment of flood defences, a case study: 17th street flood wall, New Orleans[J]. Georisk Assessment & Management

of Risk for Engineered Systems & Geohazards, 2010, 4(4): 157−173.

[20] RAVICHANDRAN N, WANG L, RAHBARI P. Robust optimization for stability of I-walls and levee system resting on sandy foundation[J]. KSCE Journal of Civil Engineering, 2022, 26(1): 57−68.

[21] DAVIDSON M, PATEV R C, CONSOLAZIO G R. Probabilistic risk assessment of barge impacts on hurricane floodwalls[J]. Journal of Performance of Constructed Facilities, 2020, 34(2): 4020010.

[22] ZHANG L, WANG L. Reliability analysis of pile-founded T-walls using the random variable method and random field method[J]. Computers and Geotechnics, 2023, 159: 105439.

[23] ZHANG L, WANG L, TURCIOS-LOVATO K. Safety assessment of pile-founded T-walls in the face of flooding hazards[C]// Geo-Congress 2022. [S. l.]: [s. n.], 2022.

[24] WANG B, JIANG W L, WANG J F, et al. The influence of infill ALC walls on the seismic performance of prefabricated PEC T-column frames[J]. Structures, 2024, 63: 106364.

[25] GAO H M, ZHOU Y J, WANG Z H, et al. Seismic response and mitigation measures for T shape retaining wall in liquefiable site[J]. Geotextiles and Geomembranes, 2024, 53(1): 331−349.

[26] KOKKALI P, TESSARI A, ABDOUN T, et al. Settlement-induced bending moments on pile-founded floodwalls[J]. International Journal of Physical Modelling in Geotechnics, 2017, 18(1): 2−20.

[27] WANG Yuan-zhan, ZHANG Lian-li, SHANG Dan, et al. A simplified calculation method for stability of inverted T-type breakwater with jackets and pile foundations[J]. Rock and Soil Mechanics, 2012, 33(6): 1839−1844.

[28] ZHANG Lian-li, WANG Yuan-zhan, SHANG Dan. Simplified calculation methods for lateral earth resistance on pile and stability of the inverse T type breakwater with jackets and pile foundations[J]. Rock and Soil Mechanics, 2013, 34(4): 1131−1139.

[29] GAN Fei, ZHENG Gang, CAO Teng, et al. Experimental study on retaining structure of alternating combination of vertical and incline steel pipe piles[J]. Chinese Journal of Rock Mechanics and Engineering, 2023, 42(5): 1175−1187.

[30] ZHANG Ming, HU Rong-hua, LIU Guo-nan. Study of relief effect of sheet pile wall with relieving platform based on model tests[J]. Industrial Construction, 2019, 49(4): 121−126, 100.